The Astronomical Journal, 129:2481–2495, 2005 May

DRIVING SPIRAL ARMS IN THE CIRCUMSTELLAR DISKS OF HD 100546 AND HD 141569A

Alice C. Quillen, Peggy Varnière, Ivan Minchev, and Adam Frank
Department of Physics and Astronomy, University of Rochester, Rochester, NY 14627; aquillen@pas.rochester.edu, pvarni@pas.rochester.edu, iminchev@pas.rochester.edu, afrank@pas.rochester.edu
Received 2003 December 23; accepted 2005 January 18

ABSTRACT

With two-dimensional hydrodynamic simulations of disks perturbed externally by stars, brown dwarfs, or planets we investigate possible scenarios that can account for the spiral structure in circumstellar disks. We consider two scenarios: spiral structure driven by an external bound planet or low-mass star, and that excited by a previous stellar close encounter or flyby. We find that both scenarios produce a morphology similar to that observed in the outer disks of HD 141569A and HD 100546: moderately open two-armed outer spiral structure. Our simulations exhibit some trends. While bound prograde objects effectively truncate a disk, a close encounter by a star instead pulls out spiral arms, spreading out the disk. Following a flyby, the morphology of the spiral structure can be used to limit the mass of the perturbing object and the time since the encounter occurred. Eccentric bound planetary perturbers tend to clear gas away from the planet more efficiently, resulting in a reduction in the excited spiral amplitude. Bound perturbers in thicker disks excite more open but lower amplitude spiral structure. When the bound object has higher mass (stellar), the disk is truncated by the Roche lobe of the planet at periapse, and each time the companion approaches periapse, spiral arms may be pulled out from the disk. Thinner disks tend to exhibit more steeply truncated disk edges. We find that the outer two-armed spiral structure at radii greater than 300 AU observed in the disk of HD 141569A is qualitatively reproduced with tidal perturbations from its companion binary HD 141569B and HD 141569C on a prograde orbit near periapse. Our simulation accounts for the outer spiral arms, but is less successful than the secular model of Augereau and Papaloizou at matching the lopsidedness or asymmetry of the disk edge at 300 AU. Our simulations suggest that the disk has been previously truncated by the tidal force from the binary and has aspect ratio or thickness $h/r \lesssim 0.1$. The simulated disk also exhibits an enhanced density at the disk edge. We find that a bound object (stellar or planetary) is unlikely to explain the spiral structure in the disk of HD 100546. A coeval planet or brown dwarf in the disk of sufficient mass to account for the amplitude of the spiral structure would be detectable in NICMOS and Space Telescope Imaging Spectrograph images; however, existing images reveal no such object. A previous encounter could explain the observed structure, provided that the disk is thin, the mass of the perturbing star is greater than $\sim 0.1\ M_{\odot}$, and the encounter occurred less than a few thousand years ago. This suggests that the object responsible for causing the spiral structure is currently within a few arcminutes of the star. However, the USNO-B proper motion survey reveals no candidate object associated with HD 100546 or any moving object that could have recently encountered HD 100546. Furthermore, the probability that a field star encountered HD 100546 in the past few thousand years is very low.

Key words: planetary systems: protoplanetary disks — stars: individual (HD 100546, HD 141569A)

Online material: color figures

1. INTRODUCTION

Recent high angular resolution studies of nearby young stars systems have revealed structure in the disks surrounding these stars. For example, gaps and holes in disks have been observed via direct or coronagraph imaging in systems such as HR 4796A and HD 141569A (Jayawardhana et al. 1998; Augereau et al. 1999a, 1999b; Weinberger et al. 1999), and intricate spiral structure has been revealed in the circumstellar dusty disks surrounding HD 100546 and HD 141569A (Grady et al. 2001; Clampin et al. 2003). These two disks are very large (outer radius a few hundred AU) and the spiral structure is suspected to be caused by a perturber external to the system, such as a recent stellar encounter in the case of HD 100546 or its companion binary, HD 141569B, HD 141569C, in the case of HD 141569A (Grady et al. 2001; Clampin et al. 2003; Augereau & Papaloizou 2004).

While HD 100546 is relatively isolated, most stars are born in embedded stellar clusters (Lada & Lada 2003). HD 141569A is in a low-density region near a molecular cloud and has three nearby young stars in its vicinity (Weinberger et al. 2000). During the time that a star is part of its birth cluster, large circumstellar disks can be perturbed by close encounters with stars (e.g., see Adams & Laughlin 2001). Many stars are part of binary systems. Consequently, the nearby stellar environment may be a key factor influencing the extent and evolution of circumstellar disks. By studying the structure observed in the largest of these disks, we hope to better understand the effect of external perturbers on these disks. We can also probe for the dependence of the spiral structure on the properties of the disk itself, thus allowing us to learn about the formation and evolution of extrasolar planetary systems.

HD 100546 is a nearby southern Herbig Be star (KR Mus; B9.5 Ve; distance $d = 103 \pm 6$ pc) with an age estimated at $t \sim 10$ Myrs (van den Ancker et al. 1997). HD 141569A (B9.5 Ve) is similar, with $d = 99 \pm 10$ pc and age $t \sim 5$ Myrs (Weinberger et al. 2000). Infrared spectroscopy with the *Infrared Space Observatory* (*ISO*) revealed solid-state emission features in HD 100546 similar to those seen in the spectrum of comet Hale-Bopp (Malfait et al. 1998; Bouwman et al. 2003). While many studies of circumstellar disks have been carried out with spectra (Hu et al. 1989; Malfait et al. 1998; Li & Lunine 2003), recent imaging studies have been able to resolve the disks

out to the large distance of 3″–6″, or 300–600 AU (Augereau et al. 1999a, 2001; Grady et al. 2001; Pantin et al. 2000; Weinberger et al. 2000, 1999). The *Hubble Space Telescope* (*HST*) STIS and ACS studies, in particular, have revealed the presence of intricate structure in these disks, including two-armed spiral structure at a radius of a few arcseconds or a few hundred AU from the star.

The opening angle is large enough that spiral structure is clearly defined in the STIS and ACS images. For HD 100546, the amplitude of the spiral structure is probably low. From the surface brightness profiles shown by Grady et al. (2001), we estimate $A = dS/S \sim 0.15$, where S is the surface brightness at optical wavelengths and dS represents the size of azimuthal variations in S. Because of the difficulty removing the residual diffracted and scattered light from the star (as discussed by Grady et al. 2001), this amplitude is uncertain. For HD 141569A, the spiral structure is high amplitude/contrast in the outermost regions, and of lower amplitude at smaller radii (Clampin et al. 2003). We note that because of the different instrument characteristics and filter bandpasses, care should be used in comparing the STIS images (HD 100546, Grady et al. 2001; HD 141569A, Mouillet et al. 2001) with ACS images (HD 141569A; Clampin et al. 2003). While the disk edge of HD 141569A is sharply defined, HD 100546 has an envelope that extends out to a radius larger than 1000 AU (Grady et al. 2001).

As suggested by Grady et al. (2001) and Clampin et al. (2003), massive external perturbers could be responsible for exciting the observed spiral structure in these circumstellar disks. Alternative possibilities include gravitational instability (e.g., Fukagawa et al. 2004) and an internal perturber such as a planet or brown dwarf (e.g., Mouillet et al. 2001). We first consider the possibility that the disk could be gravitationally unstable to the formation of spiral density waves.

The Toomre Q parameter for a gaseous disk $Q \sim c_s\kappa/\pi G\Sigma$, where κ, the epicyclic frequency at radius r, is equivalent to the angular rotation rate Ω for a Keplerian disk. Here Σ is the gas density per unit area and c_s is the sound speed (Binney & Tremaine 1987). When Q drops to near 1, the disk becomes unstable to the growth of spiral density waves. Hydrostatic equilibrium can be used to relate the disk thickness to its sound speed, $h/r \sim c_s/v$, where the disk aspect ratio is h/r, h is the vertical scale height of the disk, and v is the circular velocity. Assuming a Keplerian disk and approximating the mass of the disk $M_d \sim \pi\Sigma r^2$, we find $Q \sim (M_*/M_d)(h/r)$, where M_* is the mass of the star. From this we see that if the disk has a low density, a very thin and cold disk is required for Q to drop below 1 or 2, allowing the growth of spiral density waves in the disk. Gas densities are expected to be low in circumstellar disks. For example, when $M_*/M_d \gtrsim 100$ only an extremely thin disk, $h/r \lesssim 0.01$, would be unstable, allowing $Q \lesssim 1$. Because this aspect ratio is extreme, we must consider alternative possibilities to account for the spiral structure.

The dispersion relation for tightly wound hydrodynamic waves in a two-dimensional gaseous disk suggests that an internal perturber (such as a planet) would produce spiral arms that are more tightly wound with increasing radius from the star (e.g., Lin & Papaloizou 1993). However, the spiral arms in the disks of HD 100546 and HD 141569A are more open (less tightly wound) with increasing radius, suggesting that the force responsible is increasing with radius. This would be true if the spiral structure was caused by an external tidal force or density waves excited from an external massive body. Consequently, we consider here massive perturbers that are located exterior to the location of the spiral arms.

When a star has a close encounter with a planetesimal disk, the tidal force from the star can cause an inclination change in the outer disk (Larwood & Kalas 2001), scatter objects in an extrasolar Oort cloud analog (Kalas et al. 2001), and cause short-lived spiral structure in a gaseous disk (Pfalzner 2003; Clarke & Pringle 1993; Boffin et al. 1998; Korycansky & Papaloizou 1995). Alternatively, in the context of stellar binaries, previous studies have shown that if a secondary star is exterior to a disk, spiral density waves are driven into the disk (Artymowicz & Lubow 1994; Savonije et al. 1994). Most of the binary/disk simulations of Savonije et al. (1994) showed prominent two-armed structure similar in morphology to the outermost parts of the HD 100546 system. Tidal forces from a binary can also cause the outermost part of disk to be lopsided, as shown in the case of HD 141569A (Augereau & Papaloizou 2004).

In this paper we consider these two scenarios that could account for the spiral structure in HD 100546 and HD 141569A. We investigate the feasibility of these scenarios by carrying out hydrodynamic simulations. With these simulations we explore the types of encounters that can produce two-armed spiral structure similar to that observed in the disks of HD 100546 and HD 141569A. We aim to produce numerical simulations that exhibit two outer open spiral arms and roughly match the spiral amplitudes in the disks of HD 100546 and HD 141569A. In § 2 we describe our simulations. In § 3 we investigate the possibility that an object bound to the star, external to the disk, could tidally excite spiral structure and drive density waves into the disk. In § 4 we explore the possibility that a recent nearby stellar encounter causes the observed spiral structure. In § 5 we consider observational constraints on the possible external perturber responsible for the spiral structure in the disk of HD 100546. A summary and discussion follow.

2. SIMULATION OF SPIRAL STRUCTURE CAUSED BY EXTERNAL PERTURBERS

To determine the likely cause of the spiral structure in the outer parts of these circumstellar disks, we have carried out two series of simulations. Because we have little information about the vertical geometry and structure of these disks, we have restricted this initial study to two-dimensional hydrodynamic simulations, confining our study to the plane containing the disks.

Both planetesimal and gaseous disks can be approximated as fluid disks that are described with a sound speed and a kinematic viscosity. For planetesimal disks, the sound speed depends on the particle velocity dispersion, but for gaseous disks it is expected to depend on turbulent motions. On the basis of the images by Grady et al. (2001), we estimate that fine features in the disk of HD 100546 have widths ∼0.″3 at a radius from the star of ∼3″. The disk of HD 141569A exhibits features with widths ∼0.″6 at a radius from the star of ∼4″. The width of these features suggests that structure exists in these disks at a scale height h with vertical aspect ratio $h/r \lesssim 0.15$. However, because we may only be seeing an illuminated surface (e.g., Dullemond & Dominik 2004), these features may not be directly related to density variations in the disk. Nevertheless, if the features observed are interpreted to be in the disk, the disk is not likely to be extremely thick, $h/r > 0.2$. Consequently, we assume here that the dynamics of these disks may be approximated with two-dimensional simulations.

Scattered light optical and near-infrared imaging and thermal infrared observations show that the disks of HD 100546 and HD 141569A are dusty (Malfait et al. 1998; Bouwman et al. 2003;

Li & Lunine 2003; Augereau & Papaloizou 2004; Weinberger et al. 1999). Both disks are strongly depleted of gas; HCO+ was not detected in HD 100546 (Wilner et al. 2003), although cold CO has been detected at low levels in HD 141569A (Zuckerman et al. 1995). Gas has been detected in the inner few tens of AU in HD 100546 from UV absorption lines of atomic species and molecular hydrogen (Deleuil et al. 2004; Lecavelier des Etangs et al. 2003) and in CO and H3+ from HD 141569A (Brittain & Rettig 2002). The small dust grains detected in infrared emission from HD 141569A need to be replenished on timescales shorter than the age of the system (Li & Lunine 2003; Augereau & Papaloizou 2004); consequently, HD 141569A is most likely a young debris disk. The vertical optical depth of the disk of HD 141569A in visible wavelengths at 200 AU is low, $\tau \sim 0.024$ (Li & Lunine 2003). The disk of HD 100546 intercepts about 50% of the stellar light and emits prominently in the mid-infrared (Bouwman et al. 2003). The low level of hot dust emitting in the near-infrared, and the presence of crystalline silicate emission features, suggest that the disk is depleted at around 10 AU and flared outside this radius and that planets may have formed in the inner region (Bouwman et al. 2003). The disk is probably optically thick in visible wavelengths at 10–30 AU but may not be at larger radii (Bouwman et al. 2003). There is no direct evidence based on the modeling of the infrared spectrum that HD 100546 is a debris (rather than gaseous) disk, although Grady et al. (1997) suggested that planetesimals exist in the disk on the basis of spectroscopic variability that could be interpreted in terms of star-grazing comets.

Although the composition of these disks is not precisely known, the possible presence of planetesimals in these disks suggests that collisionless particle simulations (e.g., Pfalzner 2003; Augereau & Papaloizou 2004) might be a better match to their physical properties. Here we carry out hydrodynamic simulations rather than collisionless particle simulations. The primary advantage of the grid-based hydrodynamic simulations is that structure can be seen across a fairly large dynamic range in density. This allows us to probe structure at disk edges and resolve small differences in density due to spiral structure. To resolve low-intensity spiral structure, particularly at the edge of a disk (such as is seen in HD 141569A), or low-amplitude structure (such as is seen in HD 100546), a large number of simulated collisionless particles would be required. For younger systems such as HD 100546, which has a high optical depth, collisions could be frequent enough that particle motions are damped. Because of shocks and viscous effects, hydrodynamic simulations will damp noncircular motion. While neither purely collisionless particle simulations or hydrodynamic simulations are perfect physical models for debris disks, because we can better resolve faint or low-amplitude structure, our simulations are complementary to those carried out using simulations comprising collisionless particles (e.g., Pfalzner 2003; Augereau & Papaloizou 2004).

Both hydrodynamic and particle simulated disks support spiral structure; however, there are differences in the dispersion relation for spiral density waves. High-frequency spiral density waves (similar to sound waves) are carried by hydrodynamic disks but are damped in particle disks. In both cases the effective sound speed can be estimated using an estimate for the disk thickness and vertical hydrostatic equilibrium.

Our simulations are carried out using the hydrodynamic code developed by Masset (2002) and Masset & Papaloizou (2003). This code is an Eulerian polar grid code with a staggered mesh and an artificial second-order viscous pressure to stabilize the shocks (see also Stone & Norman 1992). The hydrocode allows tidal interaction between one or more massive bodies (planets) and a two-dimensional non–self-gravitating gaseous disk, and is endowed with a fast advection algorithm that removes the average azimuthal velocity for the Courant time step limit (Masset 2000). The simulations are performed in the noninertial nonrotating frame centered on the primary star (similar to a heliocentric frame). A logarithmic grid in radius was adopted.

TABLE 1
Numerical Simulations with Exterior Bound Planets or Stars

Simulation	q ($\times 10^{-3}$)	e	h/r
A	1	0.0	0.04
B	3	0.0	0.04
C	3	0.25	0.04
D	3	0.5	0.04
E	5	0.0	0.04
F	5	0.25	0.04
G	5	0.5	0.04
H	10	0.0	0.04
I	10	0.25	0.04
J	10	0.5	0.04
K	5	0.25	0.06
L	5	0.25	0.10
M	200	0.2	0.04
N	200	0.4	0.04
O	200	0.6	0.04
P	200	0.4	0.10

Notes.—The parameter q is the ratio of the perturber's mass to the central stellar mass, e is the planet's eccentricity, and h/r is the disk aspect ratio (setting the sound speed). For these simulations, the disk Reynolds numbers $\mathcal{R} = 10^6$. For simulations A–L, the planet's semi-major axis is at 1.2 times $R_{\max}$, the disk outer edge. For simulations M–P, the position of periapse $a(1 - e)$ is fixed at 1.1 times $R_{\max}$.

The code is scaled so that the unit length is the outer edge of the disk and the unit mass is that of the central star. Time is given in units of one orbital period for a particle in a circular orbit at the outer edge of the disk. For both HD 100546 and HD 141569A with a disk of radius ~300 AU and stellar mass of $M_* \sim 2.5\ M_\odot$, this period is $P_{\rm outer} \sim 3300$ yr.

The disk aspect ratio is defined as h/r, where h is the vertical scale height of the disk. The disk aspect ratio is assumed to be uniform and constant for each simulation. The sound speed of the gas is set from the disk aspect ratio. From hydrostatic equilibrium, we have $h/r \sim c_s/v_c$, where v_c is the velocity of an object in a circular orbit and c_s is the sound speed or velocity dispersion. The simulations are begun with a disk with a smooth and azimuthally symmetric density profile $\Sigma(r) \propto (r/R_{\min})^{-1}$, where $R_{\min}$ is the inner disk radius. Because the tidal force from the perturber can pull gas outward, we set the outer boundary to be open, allowing mass to flow outward. The grid inner boundary only allows gas to escape so that the disk material may be accreted on to the central star.

Both particle and gaseous disks exhibit viscosity. In gaseous disks, the viscosity is usual related to the α-parameter, whereas in particle disks an effective viscosity is dependent on the opacity of the disk (e.g., Murray & Dermott 1999). In our simulations, the disk viscosity is parametrized with the Reynolds number $\mathcal{R} \equiv r^2\Omega/\nu$, where r is the radius, ν is the kinematic viscosity, and Ω is the Keplerian angular rotation rate of a particle in a circular orbit of radius r. In these simulations, the Reynolds number is assumed to be constant with radius. The Reynolds number determines the timescale in rotation periods over which viscosity can cause accretion. The ages of these systems, 5–10 Myr, is only a thousand times the orbital period

TABLE 2
NUMERICAL SIMULATIONS WITH STELLAR PARABOLIC ENCOUNTERS

Simulation	q	R_a	h/r
R	0.3	0.5	0.04
S	0.1	0.5	0.04
T	0.05	0.5	0.04
U	0.1	0.5	0.10

NOTES.—Encounters are parabolic with initial starting point 1.8 times the disk outer radius. The parameter R_a is the radius of closest approach times the disk outer radius.

at the outer disk edges. Because of the short number of orbital periods comprising the lifetime of these disks, viscosity probably does not strongly affect the recent dynamics. We have chosen a Reynolds number for our simulations ($\mathcal{R} = 10^6$) that is high enough that viscous effects such as accretion should not be important during the simulations.

We ran two sets of simulations, one set for eccentric bound objects (planets or stars) and one set for stellar flybys or nearby stellar encounters. The eccentric object simulations were run with a radial and azimuthal resolution of $N_r = 150$ and $N_\theta = 450$ and the planet or star was begun initially at apoapse. The flybys were run with a resolution of $N_r = 200$ and $N_\theta = 600$, and the star was initially begun at a radius of 1.8 times $R_{\max}$ on a parabolic orbit. Table 1 shows the characteristics of the simulations with bound planets (simulations A–L) or stars (simulations M–P), and Table 2 lists those involving stellar flybys (simulations R–U). Parameters varied are the mass ratio between the perturber and central star, q; the disk aspect ratio, h/r; the eccentricity of the perturber, e, when it is bound; and the radius from the central star of the perturber's closest approach, R_a, when the perturber is on a parabolic encounter. All perturbers were assumed to be on prograde orbits.

3. BOUND EXTERNAL PERTURBERS

We consider bound external planets and bound external stars separately. Bound low-mass objects require many orbits to move material in the disk. The main mechanism for doing this is the excitation of spiral density waves at Lindblad and corotation resonances (e.g., Lin & Papaloizou 1993). However, an external star exerts such a strong tidal force that its Roche lobe can reach beyond the location of most of these resonances. Because HD 141569A has the binary HD 141569B and HD 141569C in its vicinity (Weinberger et al. 2000), we can consider the possibility that the binary is bound to HD 141569A. However, HD 100546 has no known companions. If it has a bound companion, it is probably low mass. Consequently, we divide this section into two pieces, that investigating the influence of bound low-mass companions (appropriate for HD 100546) and that investigating the influence of higher mass stellar companions (appropriate for HD 141569A).

3.1. *Bound External Planets*

In Figure 1 we show the effect of different mass planets exterior to the disk for a planet eccentricity of $e = 0.25$ (simulations C, F, and I). We see that prominent spiral structure is driven into these disks, similar to that exhibited in previous simulations of stellar binary/disk interactions (e.g., Savonije et al. 1994). For low-eccentricity, moderate-mass planets, the dominant resonance driving spiral density waves is the 2:1 or $m = 2$ Lindblad resonance, exciting in the disk two strong spiral arms. The location of the spiral arms is near the location of this Lindblad resonance or at 0.76 times the semimajor axis of the external perturber in the case of a Keplerian disk. The dispersion relation for tightly wound hydrodynamic waves in a two-dimensional gaseous disk is $\left[m(\Omega - \Omega_p)\right]^2 = \kappa^2 + k^2c^2$, where $\kappa(r)$ is the epicyclic frequency, Ω_p is the angular rotation rate of the spiral pattern, m is the number of arms, c is the sound speed, and k is the wave vector of the spiral arms. This dispersion relation ignores the self-gravity and vertical structure of the disk. As expected from the dispersion relation, the spiral structure is more open (has a higher pitch angle or lower value of k) nearing the Lindblad resonance.

While two dominant spiral arms are seen in the simulations shown in Figure 1, these two arms are not exactly symmetric. In other words, one spiral arm rotated about 180° does not lie exactly on top of the other. As explored by Henry et al. (2003) in the case of the spiral arms of M51, the interplay between different density waves provides one possible simple explanation for such a phenomenon. In these simulations we see a feature extending toward the location of the planet that rotates with the planet, and so is probably associated with the planet's corotation resonance. The asymmetries in the spiral structure are

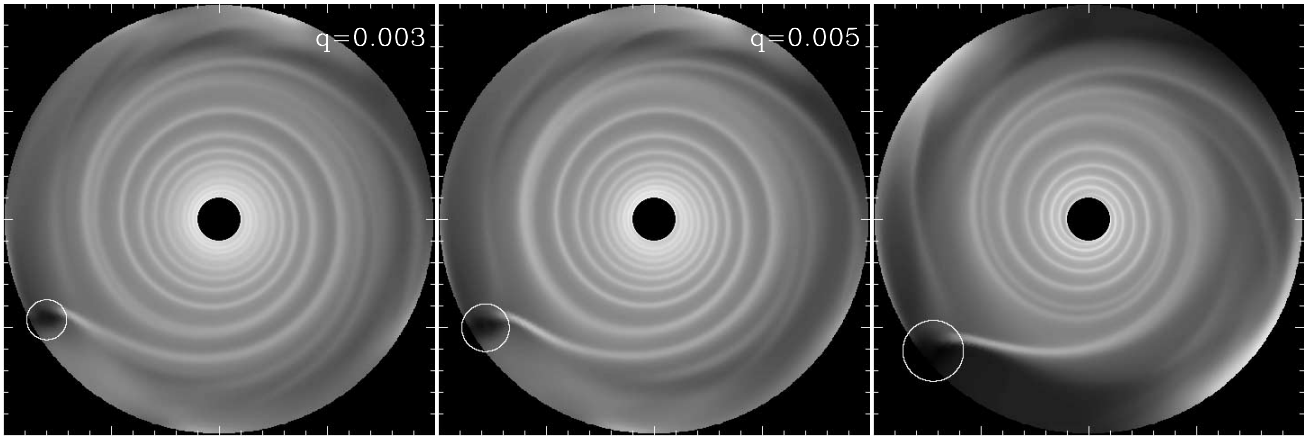

FIG. 1.—Effect of planet mass on spiral structure driven by an external planet. Simulations C, F, and I listed in Table 1 are shown. They have planet mass ratios $q = (3, 5, 10)\times10^{-3}$ (*left to right*), disk aspect ratios $h/r = 0.04$, and planet eccentricities $e = 0.25$. The Roche radius of the planet is shown as a white circle. The gas density is shown when the planet is at perihelion. The planet's semimajor axis is at 1.2 times $R_{\max}$, the disk outer edge. These simulations are shown at time $t \sim 6P_{\rm outer}$ after the beginning of the simulation, where $P_{\rm outer}$ is the rotation period at the disk outer edge.

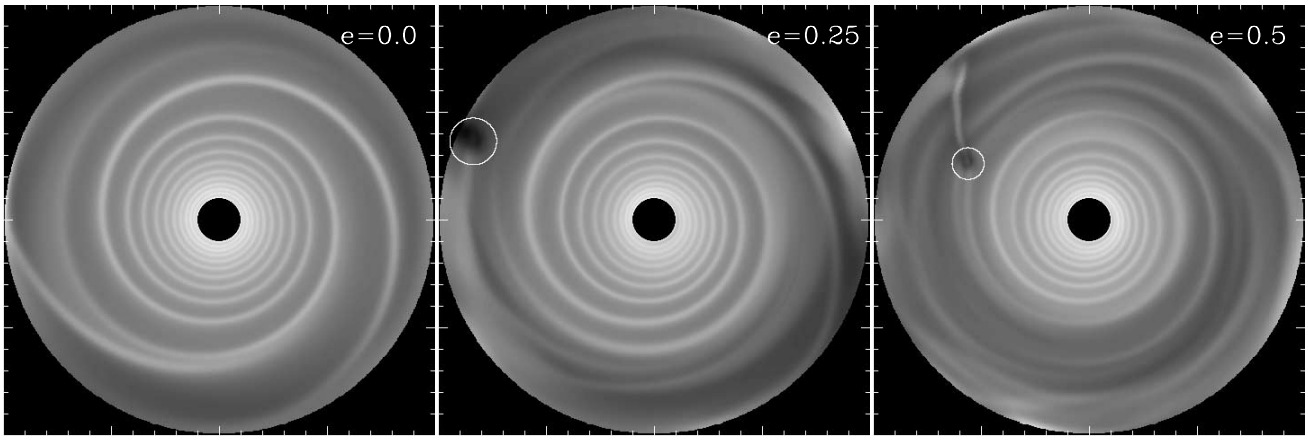

FIG. 2.—Effect of planet eccentricity on spiral structure driven by an external planet or bound star. The simulations E, F, and G are shown. They have planet eccentricities $e = 0.0, 0.25, 0.5$ (*left to right*) and aspect ratios $h/r = 0.04$. The simulations are shown at times with the planet near periapse. The planet mass ratios $q = 5\times10^{-3}$. The planet's semimajor axis is at 1.2 times $R_{\max}$, the disk outer edge. High-eccentricity planets more effectively clear gas away from the planet. Consequently, the spiral density waves driven by higher eccentricity planets are more tightly wound.

likely to be caused by the time-dependent interplay between $m = 2$ and other density waves (e.g., $m = 1$ and $m = 3$) excited by the planet. Deviations from perfect bisymmetric symmetry observed in the spiral structure of HD 100546 and HD 141569A could be explained by the interplay between spiral density waves.

When the external planet is on an eccentric orbit, because additional Fourier components exist in the perturbing potential, waves are driven at corotation resonances as well as at Lindblad resonances (Goldreich & Tremaine 1980). Consequently, we would expect stronger $m = 2$ spiral structure in the simulations containing an eccentric object (e.g., Goldreich & Sari 2003). In Figure 2 we show simulations for different eccentricity planets (simulations E, F, and G) but the same semimajor axis.

Contrary to our initial expectation, the simulations containing higher eccentricity perturbers have lower amplitude spiral structure. Examination of the simulations shows that the eccentric objects more effectively truncate the disk, in part because the perturbing object passes deeper into the disk. Nevertheless, an $m = 2$ spiral density wave is still driven into the disk, although at lower amplitude. When the perturbing object has an eccentricity above 0.23, the object passes within its 2:1 Lindblad resonance, the location where we expect that two-armed spiral density waves are excited. Since these simulations are shown at only $t \sim 6P_{\rm outer}$, we infer that the gas in the outer disk is quickly cleared away by the planet. In Figure 3 we show edge profiles corresponding to the simulations shown in Figures 1 and 2. Except for the planet in a circular orbit, the edge of the disk is within the location of the 2:1 Lindblad resonance (at $r = 0.76$). We see from Figure 3 that the position of the disk edge is more strongly dependent on the planet eccentricity (and the location of periapse) than on the planet mass.

One way to account for the lower amplitude spiral structure exhibited in the simulations containing higher eccentricity objects is with a model in which the wave is driven in low-density region at the location of the resonance (e.g., Varnière et al. 2004). Because the waves are excited in a region of lower density, the resulting amplitude of the waves is low even though there is more than one resonance responsible for driving the waves. Because the eccentric object can more effectively truncate the disk, the amplitude of the $m = 2$ waves can actually be reduced rather than increased. In Figure 2 we also note that the spiral structure in the simulations with higher eccentricity objects is more tightly wound. This is expected from the dispersion relation, which implies that the waves become more tightly wound as the distance from the resonance increases.

Figures 1 and 2 show images at time $t \sim 6P_{\rm outer}$ after the beginning of the simulation. This time period corresponds to about 2×10^4 yr and is significantly less than the age of the star. There are two effects that reduce the density of the outer part of the disk, viscous accretion that takes place on the viscous timescale, and the waves themselves, which carry angular momentum. Because these simulations have disk Reynolds numbers of

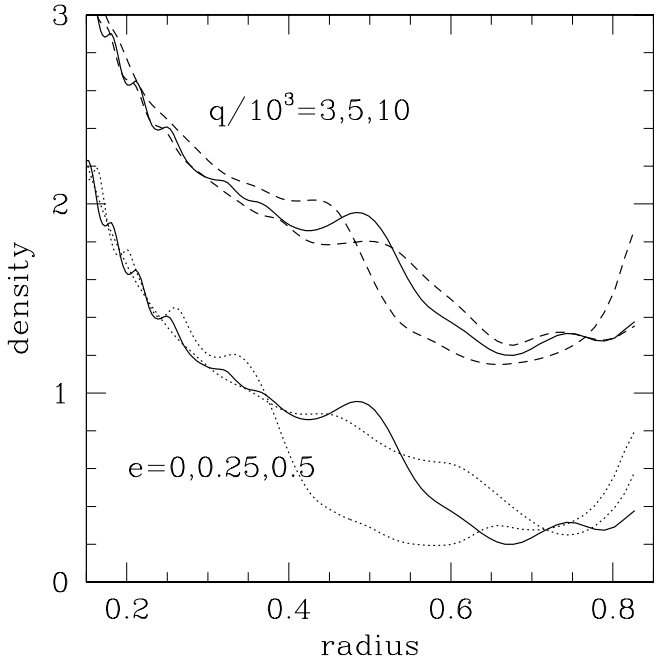

FIG. 3.—Edge profiles for the simulations shown in Figs. 1 and 2. The top three profiles show the azimuthally averaged density as a function of radius for the $e = 0.25$, $q = (3, 5, 10)\times10^{-3}$ simulations (simulations C, F, and I, respectively). These are artificially offset by a density of 1. The bottom three density profiles refer to those with $q = 5\times10^{-3}$ and $e = 0, 0.25,$ and 0.5. The two solid lines correspond to the same simulation with $e = 0.25$ and $q = 5\times10^{-3}$. We see that higher eccentricity planets truncate the disk at a smaller radius. By comparing the top three profiles with the bottom three we find that the disk edge is not as strongly dependent on the planet mass as on the planet eccentricity.

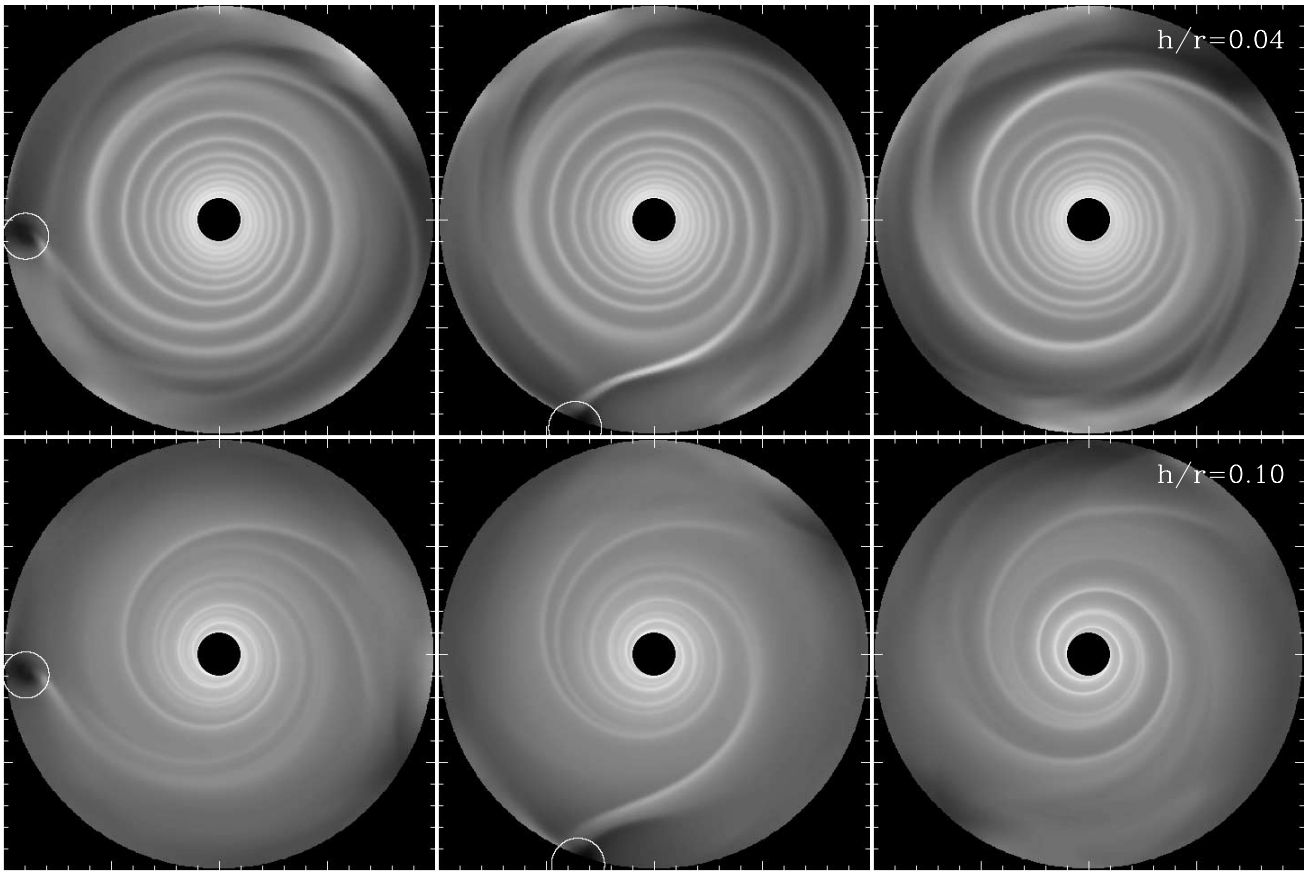

FIG. 4.—Effect of the sound speed on spiral structure driven by an external planet or bound star. Two simulations, F and L, are shown for times when the planet is at periapse (*left panels*), at apoapse (*right panels*), and at an intermediate time (*middle panels*). The planets have eccentricities $e = 0.25$ and planet mass ratios $q = 5\times10^{-3}$. The simulations shown in the top panels have disk aspect ratios of $h/r = 0.04$, and those shown in the bottom panels have $h/r = 0.10$. Thicker (or higher sound speed) disks exhibit lower amplitude and a more open spiral structure.

$\mathcal{R} = 10^6$, we do not expect to see significant accretion that takes place on a viscous timescale (10^6 times the orbital period) in our simulations, which are only run for 100–1000 orbital periods. However, the timescale for the spiral density waves to transfer material away from the planet is much shorter (Savonije et al. 1994; Varnière et al. 2004). From Figure 2 we can see that the simulations with eccentric objects are particularly effective at driving inward gas flow in the disk edge, whereas the simulations with zero-eccentricity or low-eccentricity objects accrete gas much more slowly. The disks with low-eccentricity external objects maintain their strong $m = 2$ spiral density waves to $t > 30P_{\rm outer}$ (of order 10^5 yr), whereas those with eccentric perturbers do not.

From the dispersion relation of tightly wound arms, we expect that thicker disks with a higher sound speed would exhibit more open spiral structure (as previously seen in the simulations of Savonije et al. 1994). Figure 4 shows how the disk aspect ratio (which sets the sound speed) affects the morphology. This figure shows the same simulations at different orbital phases; the leftmost panels show the perturber at periapse and the rightmost panels show the perturber at apoapse. We see from this figure that the spiral density waves excited do tend to be more tightly wound when the sound speed is lower and the disk thinner. We also find that in the larger scale height disks, the slope of the disk edge is shallower, suggesting that the resonant excitation of the spiral density waves arises from a larger region in the disk (Artymowicz & Lubow 1994; Lin & Papaloizou 1993).

From Figure 1 we see that low-mass (Jupiter sized), low-eccentricity bound perturbers can excite two-armed moderate amplitude spiral arms. This morphology is similar to that exhibited by the disk of HD 100546. Because of the short timescale (a few rotation periods at the outer edge of the disk) in which gas is cleared to within the 2:1 Lindblad resonance, strong observed open two-armed spiral structure as seen in the disk of HD 100546 is unlikely to be excited by a highly eccentric ($e \gtrsim 0.20$) bound planetary perturber. On a timescale of a few rotation periods, the edge of the disk moves sufficiently away from the perturber that strong open two-armed structure is no longer evident.

We now compare the morphology of the simulations to that seen HD 100546. The disk of HD 100546 exhibits two arms that are more open at larger radii than at smaller radii. The simulated disks shown in Figure 1 also show spiral structure that is more open at larger radii and more tightly wound at smaller radii. The simulations also show more tightly wound structure at smaller radius, which is not detected in the image of HD 100546. This could in part be because of the increased level of light from the central star, which would make it difficult to detect fine structure in the disk. Alternatively, the disk of HD 100546 may comprise planetesimals; a particle disk would damp tightly wound waves. For objects on circular orbits, we find that the amplitude of the waves drops below about 15% (as observed for HD 100546), when the mass ratio $q \lesssim 0.005$. If a bound perturber is responsible for the spiral structure in the disk of HD 100546, our simulations suggest that the perturber must have mass above

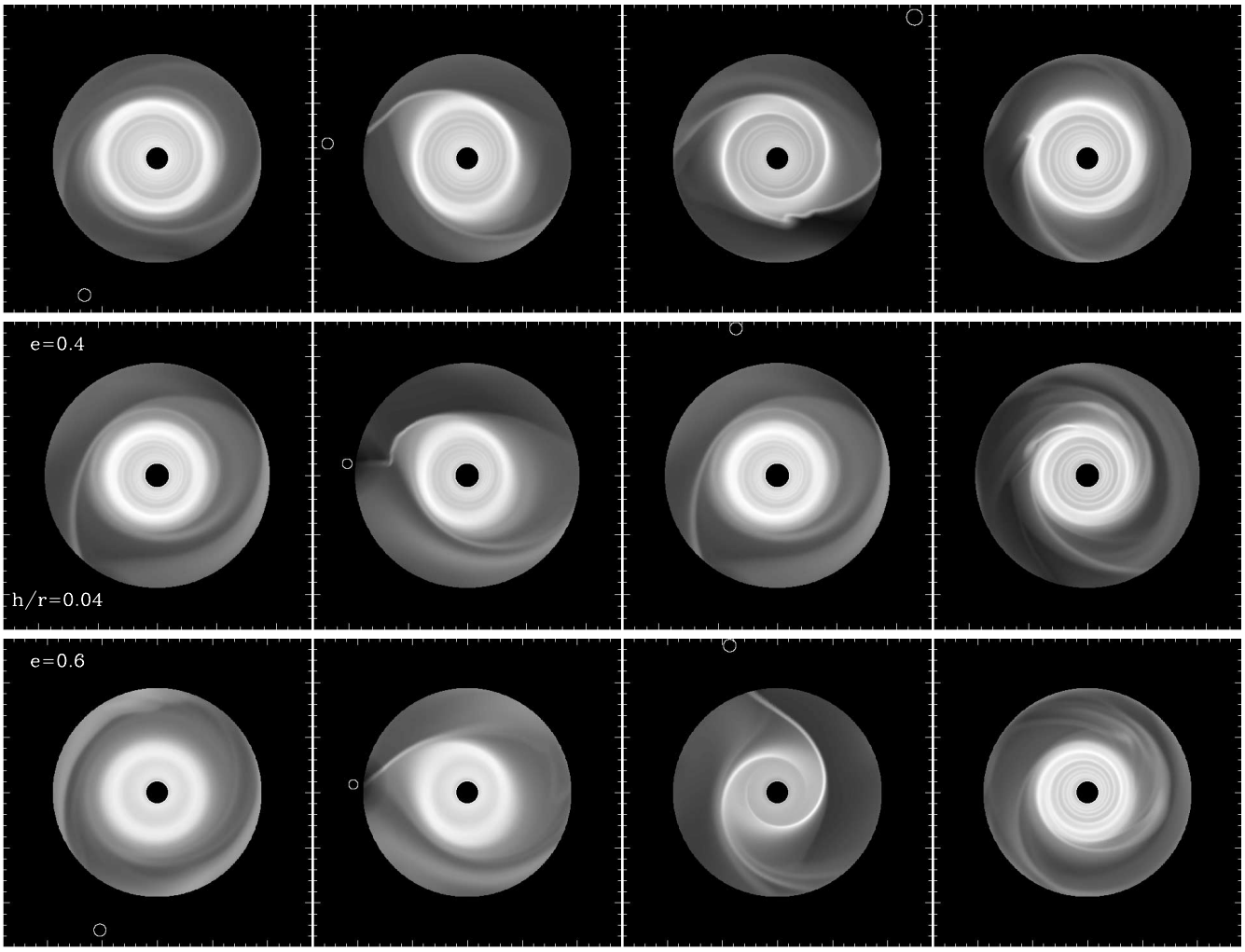

FIG. 5.—Role of eccentricity in the disk morphology for external bound stellar-mass companions. These simulations (M, N, and O) have mass ratios $q = 0.2$ and disk aspect ratios $h/r = 0.04$. The position of periapse is approximately 1.1 times the outer disk radius in all simulations. The top panels have perturber eccentricities $e = 0.2$, the middle panels $e = 0.4$, and the bottom panels $e = 0.6$. Left to right, each panel shows simulations just before periapse (*left*), at periapse, after periapse, and nearly at apoapse (*right*). The small circles show the location of the perturber. Just following periapse, asymmetric spiral arms are pulled out of the disk. The perturber truncates and compresses the disk, enforcing a higher gas density near the edge and a sharper edge profile. Spiral density waves driven into the disk cause elevated accretion episodes in the disk interior.

$10M_J$. If the disk is thicker, a higher mass perturber would be required. We use these limits in § 4 when we discuss observational constraints on these scenarios.

3.2. *Bound External Stars*

For HD 141569A, the likely perturber is the companion binary HD 141569B, HD 141569C, consisting of an M2 and an M4 star, located 9″ away from HD 141569A (Weinberger et al. 2000; Augereau & Papaloizou 2004). We estimate a mass ratio for the binary compared to HD 141569A of $q \sim 0.2$ on the basis of the low-mass stellar models by Baraffe et al. (2002) and the effective temperature scale by Luhman et al. (2003), consistent with $q = 0.2$ adopted by Augereau & Papaloizou (2004). The amplitude of the outer spiral structure (at radii greater than 300 AU) in the disk of HD 141569A is much higher than that of HD 100546, and the nearby binary provides a likely candidate responsible for driving it. However, $q = 0.2$ is well above the mass ratios considered for the previous simulations. To explore the way that spiral structure could be excited in the disk of HD 141569A, we ran a set of simulations with a higher mass external bound perturber with $q = 0.2$ (see Table 1).

In Figure 5 we show simulations for different binary eccentricities (M, N, and O). Simulations M and N are shown approximately 5.5 binary orbital rotation periods (BC about A) after the start of the simulation, and simulation O is shown approximately 4.5 orbital rotation periods after the start of the simulation. It is computationally expensive for us to run finely gridded hydrodynamic simulations for significantly longer time periods. The disk is truncated by the binary on its first few passages, but each subsequent close encounter excites spiral structure. The size of the disk is consistent with truncation at the Roche radius of the binary when the binary is at periapse. Consequently, the disk outer edge is well within the location of the binary's 2:1 Lindblad resonance. We see in the simulations that, following the first few passages, the disk outer edge has much higher density than the initial disk density. The binary has not only truncated the disk and induced a sharp outer edge but has also compressed it. The high edge density could be seen as a ring of material, and the lack of gas interior to the ring (e.g., Clampin et al. 2003) might be mistakenly interpreted as evidence that material has been cleared out by another process, such as an interior planet.

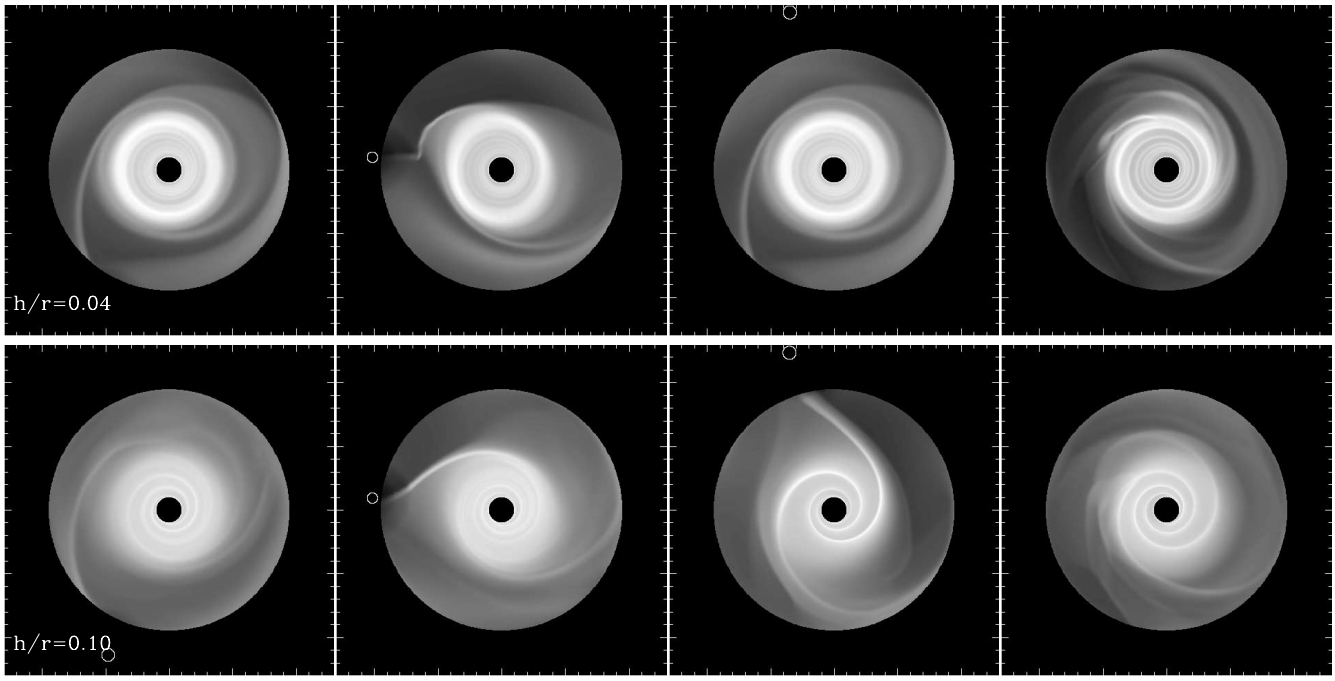

FIG. 6.—Role of disk thickness for external bound stellar-mass companions. These simulations have mass ratios $q = 0.2$ and perturber eccentricities $e = 0.4$. The disk aspect ratios are $h/r = 0.04$ for the top panels (simulation N) and $h/r = 0.1$ for the bottom panels (simulation P). Left to right, each panel shows simulations just before periapse (*left*), at periapse, after periapse, and nearly at apoapse (*right*). The disk edge profile is smoother when the disk is thicker and the spiral structure is more open.

Observations of HD 141569A suggest that the disk is cleared between 150 and 200 AU (Mouillet et al. 2001). Clearing at these inner radii is probably not caused by the perturbations from the binary HD 141569B, HD 141569C, and so is probably induced by internal processes, such as planets (see discussion by Mouillet et al. 2001). The inner boundary of our simulation is sufficiently distant from the truncated edge that it should not have affected the outer disk structure. Spiral waves driven in these simulations are damped before they reach the inner regions of the simulated disk. Hence, the presence of the clearing at 200 AU should not be able to strongly affect the morphology observed in the outer disk at 300–450 AU.

In Figure 5 we show panels preceding and following the binary's periapse. Before periapse, we see that the disk is nearly axisymmetric and is quiescent. It lacks strong spiral structure. However, at periapse the tidal force from the binary begins to pull two arms from the disk. Since one arm is directly excited by the binary and the other is excited by the recoil of HD 141569A (Pfalzner 2003), there is an asymmetry between the spiral arms. The disk is lopsided when the binary is near periapse. The asymmetric spiral structure, the lopsided disk, and the spiral arm pointing toward the perturber are features that are exhibited by the disk of HD 141569A, as seen in scattered light (Augereau et al. 1999b; Clampin et al. 2003). We find that outer spiral arms are less strongly excited by a binary on a more highly eccentric orbit. This is likely because the binary on a higher eccentricity orbit is moving somewhat faster at periapse than one at a lower eccentricity, resulting in a weaker impulse.

We investigate the role of disk thickness by displaying in Figure 6 two simulations (N and P) that differ only in the disk aspect ratio. The outer spiral arms excited by the encounter with the binary are more open in the thicker disk; however, the amplitude of the features is lower, particularly in the inner region. Also, the outer arms point directly toward the binary, rather than leading the binary as is seen in HD 141569A.

We found the closest correspondence between the observed morphology and that seen in the simulations with binary eccentricity $e \sim 0.2$, a thin disk ($h/r \sim 0.04$), and binary approaching periapse (simulation R). This simulation is shown in Figure 7 along with the observed morphology pointed out by Clampin et al. (2003). We support the scenario proposed by Augereau & Papaloizou (2004) in which the disk structure is influenced by perturbations from the binary. Our simulation is successful at producing open and high-amplitude two-armed spiral structure at the outer edge of a sharp disk, similar to that observed in the *HST* images at radii greater than 300 AU. It successfully accounts for the disk truncation. The simulation also exhibits some asymmetries that are similar to those observed. The simulated northern spiral arm is not 180° away from the southern spiral arm, but shifted or rotated westward so it is closer to the binary than it would be if it were an image of the southern spiral arm rotated by 180°. The simulated disk edge is lopsided, with the northern edge thicker and more distant from the star than the southern edge. However, the observed disk edge is brighter on the southwestern side than on the northeastern side, and this brightness difference is not seen in our simulation. The northern spiral arm is farther east and the southern arm is farther west in the simulations than the observed ones.

While we have attempted to match the outermost structure of the disk, Augereau & Papaloizou (2004) concentrated primarily on the structure of the disk edge. Our simulation accounts for the outer spiral structure, but is less good at matching the asymmetry or lopsided appearance of the bright rim of the disk. This asymmetry was well modelled with the secular model of Augereau & Papaloizou (2004), although their simulations did not exhibit the outer spiral arms that are evident in our simulations. Augereau & Papaloizou (2004) and our simulation also differ in the predicted location of the binary periapse. Our simulation has the binary periapse near the current location of the binary HD 141569B, HD 141569C, whereas Augereau &

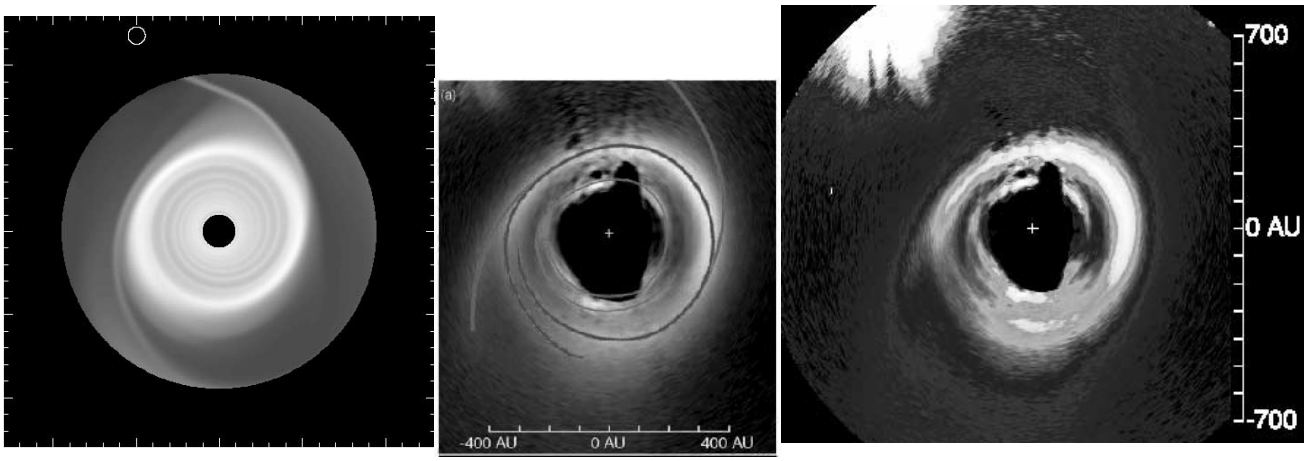

FIG. 7.—Comparison between a simulation with $q = 0.2$, $h/r = 0.04$, and $e = 0.2$ (simulation R), with the binary companion HD 141569B, HD 141569C near periapse on a prograde orbit, and the observed morphology of HD 141569A. The images in the middle and on the right are from Clampin et al. (2003). Our simulation does a reasonable job of accounting for the outer spiral structure and the location of the disk edge, matches reasonably well the position of the binary (denoted with a white circle), and predicts an asymmetry in the location of the outermost two arms that is seen in the disk of HD 141569A. Much of the structure of the outer disk may have been excited by the tidal force of the binary HD 141569B, HD 141569C. However, our simulation fails to exactly match the shape of the outermost spiral features and the lopsided nature of the disk. We suspect that a better three-dimensional simulation would be required to do this. The images of HD 141569A are shown with north to the left and west on top as by Clampin et al. (2003) and Augereau & Papaloizou (2004). [*See the electronic edition of the Journal for a color version of this figure*.]

Papaloizou (2004) suggest that the periapse is at position angle $\sim -130^\circ$, or on the southwestern side of the disk.

To account for the outer spiral arms, we have assumed that the binary is in a prograde orbit. A prograde encounter allows open high-amplitude spiral arms to be drawn out of the disk when the binary is near periapse. To truncate the disk, a much closer periapse would be required, with a retrograde orbit for the binary. Retrograde encounters are also much less effective at pulling out spiral arms near closest approach. The model of Augereau & Papaloizou (2004) did not specify whether the binary was on a prograde or retrograde orbit. Periapse is on the southwestern side of the disk in their model, so the binary is either post-periapse and retrograde or pre-periapse and on a prograde orbit. Since the phenomena they illustrate and describe in the disk was caused by secular perturbations, the direction of the binary orbit may not be important in their model. Our simulations suggest that much of the outer structure in the disk is transient and excited specifically by the current close encounter. We find that two-armed open spiral arms are best excited just past periapse for a prograde binary orbit. This presents a problem for the model of Augereau & Papaloizou (2004), since neither possibility (post-periapse and retrograde or pre-periapse and prograde) would be capable of exciting the outer spiral structure. Modifications of the secular model of Augereau & Papaloizou (2004) will be required to account for the outer spiral structure. We note that the outer spiral arm connecting the HD 141569A disk to the stellar companions was only barely detected in the images presented by Clampin et al. (2003), whereas that on the north was detected by both Clampin et al. (2003) and Mouillet et al. (2001). If future observations fail to confirm the presence of the southern arm, then a different scenario or very different orbital parameters would be required to account for only the northern arm.

Our simulation does exhibit some lopsidedness in the disk, even though the binary eccentricity we adopted was not as high as that adopted by Augereau & Papaloizou (2004). The simulations of Augereau & Papaloizou (2004) found that a highly eccentric binary was required to account for the disk asymmetry (Augereau & Papaloizou 2004) on long timescales. We found that a binary on a more eccentric orbit excited slightly more asymmetry in the disk near periapse. However, the disk tended to be offset toward the perturber rather than toward the west, as observed Mouillet et al. (2001). In our simulations, the asymmetry damps as the binary recedes following periapse. The hydrodynamic simulations explored here are unlikely to maintain the elliptical orbits exhibited by the particle simulations of (Augereau & Papaloizou 2004). It is possible that a particle simulation would provide a better match to the physical state of the disk on longer timescales than our hydrodynamic simulation. Our simulations exhibit weak spiral waves driven inside 200 AU that are not observed in the observed images of HD 141569A. Because they are tightly wound, they are similar to sound waves, and would not be present if the disk comprises planetesimals.

While our simulation provides a reasonable match to the observed outer morphology, we found previously that lower eccentricity binaries and colder disks exhibit higher amplitude and finer structure in the disk. This degeneracy makes it difficult for us to finely discriminate between models and so estimate the eccentricity of the binary's orbit. While we find a somewhat better correspondence between the simulations and observed outer spiral arm morphology with a lower eccentricity binary and relatively thin disk, we cannot exclude the possibility that the binary could have a higher eccentricity, as suggested by Augereau & Papaloizou (2004).

The chosen simulation, R, shown in Figure 7, predicts the outermost two spiral arms, matches reasonably well the position of the binary, accounts for the steep disk edge profile, and predicts an asymmetry in the outermost two arms that is seen. However, we fail to exactly match the shape of the outermost arms and the structure in the disk edge. Our previous figures showed that this issue cannot be resolved with a binary with higher eccentricity or with a thicker disk because these simulations tend to have less well defined inner disk structure, although because of the degeneracy between binary eccentricity and disk thickness we cannot tightly constrain both quantities. We note that our simulations were carried out in two dimensions, and it is likely that the binary is not exactly in the same plane as the disk of HD 141569A. The worst discrepancies between our simulations and the observed disk would be in the

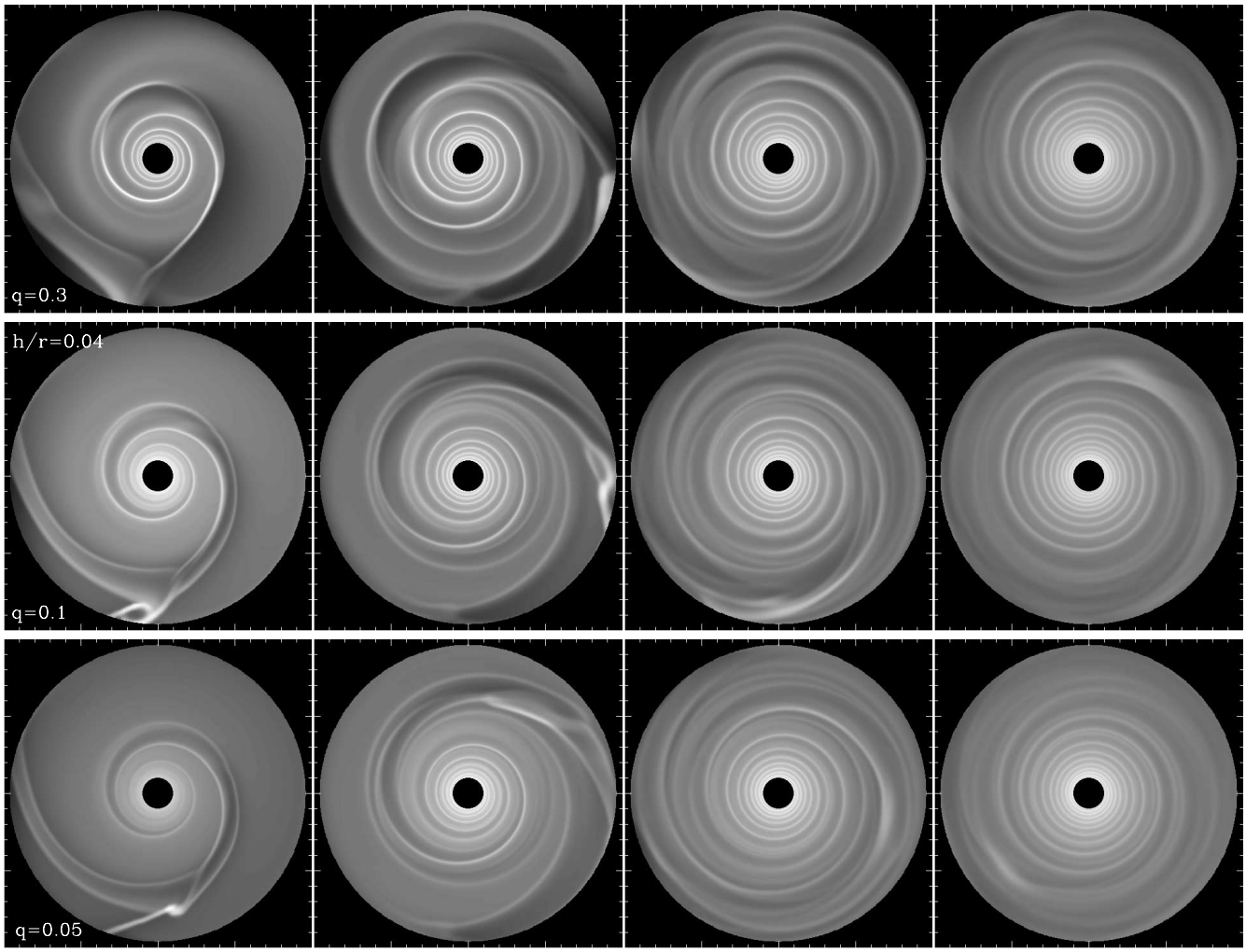

FIG. 8.—Effect of stellar mass on spiral structure excited by a recent stellar encounter. Simulations are shown at $t = 1/4, 1/2, 1, 2$, and 4 times $P_{\rm outer}$ (the rotation period at the disk outer edge) from left to right after a star of mass ratio $q = 0.3, 0.1$, and 0.05 undergoes its closest approach to the central star. Each row corresponds to a simulation with a different mass ratio (simulations R, S, and T, respectively). The position of closest approach is half the radius of the disk outer edge, and the star is assumed to be on a parabolic trajectory. For these simulations, the disk Reynolds numbers $\mathcal{R} = 10^6$ and the disk aspect ratios $h/r = 0.04$. If the perturber's mass is below $\sim$0.1 times that of the star, only one spiral arm is dominant. The short timescale of the excited spiral structure places a limit on the proximity of a perturber that could have been responsible for driving the spiral structure in the disk of HD 100546. As a guideline, the edge of the disk should be compared to the size of the disk of HD 100546, or $\sim$300 AU.

outer regions, where the tidal force from the binary on the disk is largest. By carrying out three-dimensional simulations, it may be possible to more exactly match the morphology and so more tightly constrain both the thickness of the disk and the eccentricity of the binary orbit from the disk's morphology. We have assumed here that a hydrodynamic simulation provides a good approximation to the disk of HD 141569A. However, if this disk is a debris disk, particle simulations that include collisions might provide a better physical model.

Assuming that the binary HD 141569B, HD 141569C is at periapse and an eccentricity of 0.2, the period of the orbit is a few thousand years. On the basis of an age estimate of 5 Myrs for this system, we estimate that a few thousand orbits could have occurred since the birth of the system. Augereau & Papaloizou (2004) inferred a high orbit eccentricity on the basis of the timescale for the maintenance of a lopsided disk. If the orbit of the binary is stable, then many periapse encounters could have taken place, particularly if the binary is not on a highly eccentric orbit. While a few periapse encounters are required to truncate the disk, we expect that repeated encounters could more strongly truncate the disk. As the disk decreases in size, the binary would pull out fainter and fainter arms from the edge of the disk of HD 141569A. Nevertheless, we have proposed here that the outer spiral arms observed in the disk by Clampin et al. (2003) are the result of tidal excitation from the binary HD 141569B, HD 141569C. We note that the wide separation of HD 141569B, HD 141569C from HD 141569A implies that this system may eventually be disrupted altogether by the passage of field stars. The probability of such a field star perturbing the HD 141569A, HD 141569B, HD 141569C system can be estimated as $P \sim nvA\Delta t$, where n is the number density of stars ($\sim$10 pc^{-3}), v is the field star velocity dispersion or $\sim$10 km s^{-1}, A is the cross section of the binary orbit [$\sim\pi$(1000 AU)^2], and Δt is the timescale (similar to the age of the system). On the basis of these quantities, we estimate that the HD 141569A, HD 141569B, HD 141569C system has a probability of $\sim$5% of a field star encounter during the lifetime of the system. If the binary is on a more highly eccentric orbit then the probability would be higher. One interesting possibility is that the disk of HD 141569A has only recently been truncated by the binary orbit. If the binary is on

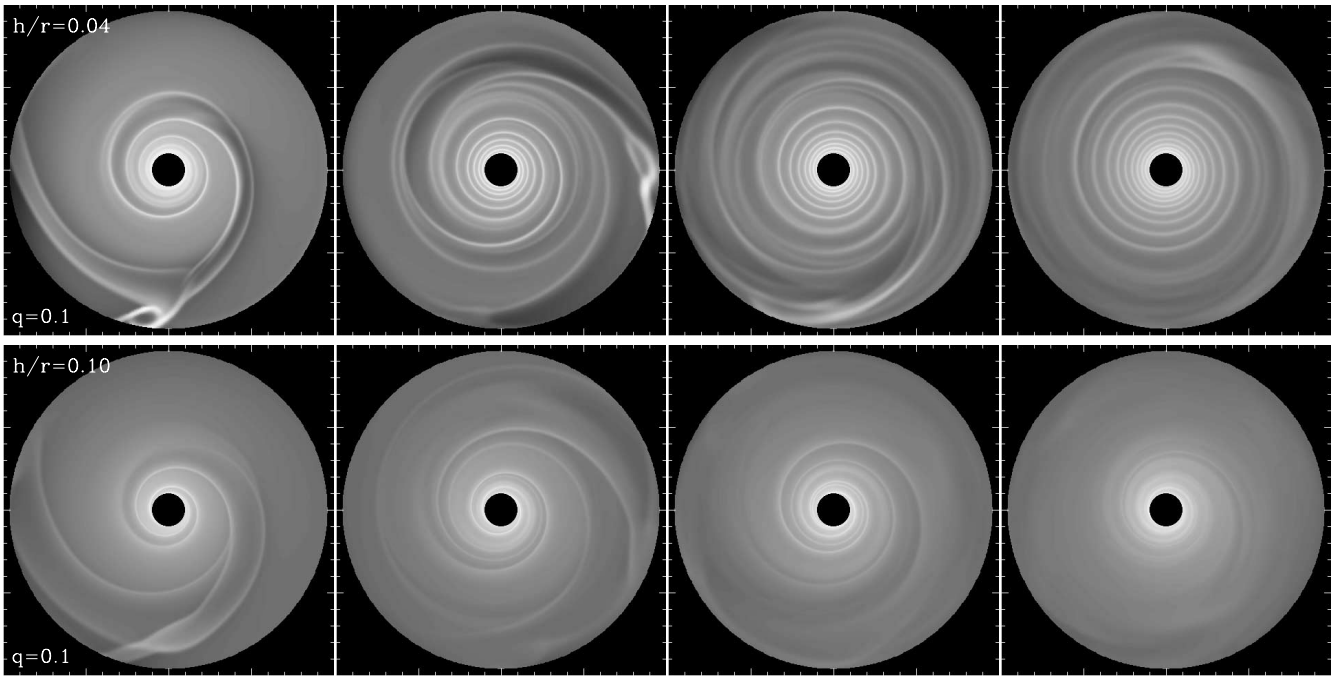

FIG. 9.—Effect of disk thickness on the morphology of spiral structure excited by a recent stellar encounter. The top panels show a simulation with disk aspect ratios $h/r = 0.04$ (simulation S) compared with that with $h/r = 0.10$ (simulation U), which is shown in the bottom panels. Left to right, each panel corresponds to a different time after the closest approach (with times the same as those in Fig. 8). For these simulations, the mass ratios $q = 0.1$. Thicker disks exhibit lower amplitude and less long lived prominent spiral structure following a flyby.

an eccentric orbit, its orbit could have been perturbed by a nearby field or birth cluster star.

3.3. *Excitation of Spiral Structure by Flybys*

In this section we consider stellar encounters as possible causes for spiral structure in circumstellar disks. This is relevant for HD 100546, which does not have any known nearby companions (Grady et al. 2001).

In Figure 8 we show simulations for parabolic stellar flybys as a function of time after the closest approach. Figure 8 shows simulations for stellar mass ratios of $q = 0.3, 0.1$, and 0.05; simulations R, S, and T, respectively. We ran these simulations so that the star passed well within the disk to minimize the effect of the outer boundary. Nevertheless, at late times the disk is clearly affected by shocks associated with the outer boundary. Our code is complementary to previous studies because it is good at showing spiral structure, but not as accurate as *N*-body or smoothed particle hydrodynamics (SPH) codes at modeling elongated tidal arms (as simulated by Pfalzner 2003; Boffin et al. 1998). Initially, the gas disk in our simulations exhibits a global two-armed spiral. The size of the secondary arm initially appears to depend on the mass ratio, although at later times the morphology is less asymmetric or lopsided. Pfalzner (2003) showed that the secondary arm is dependent on the recoil of the central star, and our simulations show the same dependence. Since HD 100546 exhibits two arms, the perturber (if a flyby) probably did not have a small mass ratio. From our simulations, we estimate $q \gtrsim 0.1$, corresponding to $M \gtrsim 0.2\ M_{\odot}$, since lower mass perturbers fail to excite two strong spiral arms.

After four rotation periods (at the outer disk edge), little strong spiral structure remains. This short timescale is consistent with the results of previous simulations (Pfalzner 2003), and allows us to place limits on the time since the closest approach. The spiral structure HD 100546 is likely to have been excited less than one rotation period (at the outer disk edge) ago, which is less than 3000 yr ago based on the rotation period at the edge of the disk of HD 100546. For an object traveling at 10 km s^{-1}, this would correspond to a distance on the sky of 1′.

Since the pitch angle and wave travel time depend on the disk sound speed, we ran a comparison simulation with $h/r = 0.1$ (simulation U) that is shown in Figure 9. We see that the amplitude of the spiral density waves is reduced in the thicker disk, even though they are more open. Because the amplitude of the spiral structure is lower, a higher mass perturber that encountered HD 100546 more recently would be required to account for the observed spiral structure.

In Figure 10 we show a comparison between an encounter and the observed morphology of HD 100546. The simulation is shown about 3000 yr ($t = 1P_{\rm outer}$) after the encounter for a mass ratio $q = 0.3$ and with disk aspect ratio $h/r = 0.04$ (simulation R). The simulation exhibits an asymmetry in the spiral structure similar to that observed, although the easternmost spiral arm is not as open as the observed one. This figure demonstrates that it is easy (and so not particularly meaningful) to simulate spiral structure similar to that observed in the disk of HD 100546. We must identify the actual object responsible for exciting the spiral structure to constrain this scenario further.

4. OBSERVATIONAL LIMITS ON THE PERTURBING OBJECT HD 100546

As discussed by Grady et al. (2001) and Augereau et al. (2001), the STIS, NICMOS, and ADONIS observations strongly constrain the types of nearby objects that could be associated with HD 100546. The nearby point sources detected in the STIS images are all too blue to be associated with the HD 100546 system, and so are likely to be background stellar sources (Grady et al. 2001). This puts strong limits on both of our scenarios. If a flyby caused the spiral structure, then the object responsible must

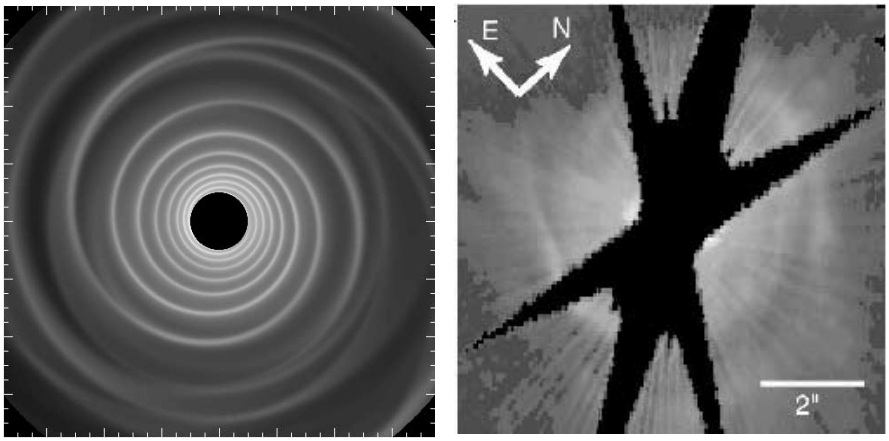

FIG. 10.—Comparison between a flyby simulation with $q = 0.3$, $h/r = 0.04$ (simulation R) and the observed morphology of HD 100546. The simulation is shown about 3000 yr after the encounter. The image on the right is the STIS image by Grady et al. (2001). As long as the perturber is $\gtrsim$0.1 times the mass of the star, two arms will be excited. The pitch angle of the arms is related to the time since the perturber reached periapse. We have found that many simulations are capable of exhibiting open two-armed structure similar to that seen in the disk of HD 100546. To constrain the nature of the excitation, it is necessary to identify the object responsible for the excitation. A flyby excites short-lived spiral structure and need not sharply truncate the disk. [*See the electronic edition of the Journal for a color version of this figure.*]

be outside the field of view of the STIS image ($\gtrsim$20″ away from HD 100546). Alternatively, if a low-mass bound object causes the spiral structure, then the mass required to excite the spiral structure must be low enough so that it would not have been detected in the existing images. Our simulations suggest that a bound mass at least as large as 0.01 times the mass of the star is needed to match the amplitude of the spiral structure. This would correspond to a mass of 0.02 $M_\odot$, or 20M_J (see § 3.1).

The division between bound perturber and flyby is important. A bound perturber will make more than one encounter over a timescale of a few thousand years. Since a first encounter disrupts the disk, the remaining disk may not exhibit strong spiral structure during subsequent approaches. Since a flyby disrupts a previously quiescent disk, strong outer spiral structure can be excited; but it would be transient, only lasting a few thousand years. Afterward, the disrupted disk could extend well past the pericenter of the encounter.

The lack of detected associated objects (point sources) in the NICMOS and STIS images can be used to estimate an upper limit on the mass of possible objects near HD 100546. The models of Baraffe et al. (2002) predict that 5M_J and 10M_J mass objects that are 10 Myr old have absolute H magnitudes of 15.3 and 11.8, respectively. These correspond to H magnitudes of 20.3 and 16.8 for objects at the distance of HD 100546. The NICMOS image of Augereau et al. (2001) detected a star of H magnitude 16.1 at a distance of 4″ from HD 100546, suggesting that objects somewhat fainter could have been detected nearer HD 100546. The disk brightness drops to 17.5 mag arcsec^{-2} in the H band at a radius of 3″ from the star (Augereau et al. 2001). Considering the NICMOS point-spread function, a star of magnitude 19–20 could have been detected against the disk at a radius of 3″ from the star.

If we adopt 10M_J (0.01 $M_\odot$) as a limiting mass for a coeval object that could have been detected in the STIS and NICMOS imaging to a radius of 3″, then we can limit the possible bound companions of HD 100546 within ~300 AU to a mass ratio $q \lesssim 0.005$.

The perturber mass limit suggested by the simulations, $M > 0.02\ M_\odot$ is in contradiction to the limits placed on possible companions by the lack of associated objects detected in *HST*/STIS and NICMOS observations. We conclude that a bound low-mass companion is not a good explanation for the observed spiral structure in the disk of HD 100546.

We now consider observational constraints on objects that could have previously encountered HD 100546. USNO-B1.0 is an all-sky catalog complete to a visual magnitude of 21 that presents positions accurate to 0.″2 and proper motions measured across 50 yr of photographic sky surveys (Monet et al. 2003). In the vicinity of HD 100546 (within 2′), the USNO-B catalog (using surveys during 1976, 1984, and 1991) yields one nearby object with a similar proper motion to HD 100546, USNO-B1.0 ID 0197-0270043, that is 54″ away from HD 100546. This star, with $M_R = 17.4$, does not coincide with any Two Micron All Sky Survey (2MASS) object, and it is quite blue ($B - R \sim 0$), suggesting that it is a white dwarf rather than a low-mass main-sequence star. Consequently, it is unlikely to be the same age as HD 100546 and so is unlikely to be associated with the star. Inspection of the USNO-B digitized images suggests that the proper motion is uncertain because of two nearby stars, one of which does have a 2MASS counterpart.

We also searched the USNO-B1.0 catalog for objects that might not be associated with HD 100546 but could have intersected the path of this star on the sky. We find no moving candidates that are red enough to be at the same distance as HD 100546 from us and that could have approached (within 15,000 AU) the path of HD 100546 in the past 9000 yr. Both the 2MASS and USNO-B catalog contain numerous red faint sources within a few arcminutes of HD 100546 that could either be candidates for low-mass stellar bound companions or low-mass stars that could have encountered the star in the past few thousand years. We failed to find an extremely red object that was seen in 2MASS (limiting magnitude $K \sim 15$) and was not seen in the USNO-B surveys (limiting magnitude $V \sim 21$). The 2MASS point source catalog contains 23 stars with near-infrared color $J - K > 0.9$ within 2′ of HD 100546. These are candidate low-mass main-sequence stars at the distance of HD 100546 lacking measured proper motions from the USNO-B catalog. Our failure to find a catalog candidate for the object responsible suggests that it must be a low-mass object. Stars later than M6 at the distance of HD 100546 (100 pc) would not be visible in the USNO-B surveys. Brown dwarfs at the distance of HD 100546 would not be seen in the 2MASS survey.

The low proper motion of HD 100546 with μR.A. $= -38$ mas yr^{-1} and μdecl. $= -2$ mas yr^{-1} makes it difficult to pinpoint faint stars at the same proper motion using ground-based data across only a 15 yr baseline (USNO-B1.0 is based on surveys in 1976, 1984, and 1991 in this region), during which time HD 100546 would have moved by only 0.″6.

Stellar collisions or flybys in the field are unlikely (e.g., Kalas et al. 2001). Assuming a stellar density of 10 stars pc^{-3} and a stellar velocity dispersion of 10 km s^{-1}, typical of the Milky Way density in midplane, and a cross section of $\pi(600\ \mathrm{AU})^2$ for the disk of HD 100546, we would estimate a probability of 0.03 that a low-mass star could have approached within 600 AU of HD 100546 in the past 10 Myrs. The probability is only 3×10^{-6} that a field star approached HD 100546 in the past 10,000 yr, the upper limit on the time since the encounter that we have inferred on the basis of the morphology of the spiral structure. However, the birth cluster of HD 100546 may have provided a denser stellar environment, increasing the probability of a stellar collision (Kalas et al. 2001; Adams & Laughlin 2001). As pointed out by Vieira et al. (1999), HD 100546 is located just to the southeast of the dark filament DC 296.2-7.9. Through their study of the extinction in this cloud, Vieira et al. (1999) and Corradi et al. (1997) find that this cloud is likely to be just past HD 100546, 110–130 pc away, and so could be associated with HD 100546. The statistics of star colors in the region suggest that a moderate minimum extinction of $A_V \sim 0.5$ is provided by the cloud (Vieira et al. 1999). From inspection of 2MASS images near HD 100546, we find no obvious stellar cluster associated with the dark filament. Unless a region of higher stellar density is found within a few arcminutes of HD 100546, the encounter would have been an exceedingly improbable and exceptional event.

5. SUMMARY AND DISCUSSION

In this paper we have used two-dimensional hydrodynamic simulations of disks perturbed externally by stars or planets to investigate possible scenarios that can account for the outer spiral structure observed in the circumstellar dusty disks of HD 100546 and HD 141569A. We consider two types of external perturbers; those in orbit about the central star containing the disk and those involving a recent stellar encounter or flyby. Both scenarios produce morphology similar to that observed, a moderately open two-armed spiral structure.

Our simulations exhibit some trends. Thicker disks tend to have lower amplitude and more openly wound spiral density waves. Eccentric planetary perturbers clear gas away from the perturber more efficiently. At earlier times in the simulations, eccentric planetary perturbers excite strong and open spiral structure; however, after a few rotation periods the edge of the disk moves inward, the waves excited become more tightly wound, and the amplitude drops. The two-armed structure excited tends to be asymmetric, a phenomenon we attribute to the interplay between $m = 2$ and additional spiral density waves at different angular rotation rates that are also excited by the perturber.

When the bound object has higher (stellar) mass, the disk is truncated at the Roche lobe of the companion. Each time the companion approaches periapse, tidal arms can be pulled out from the disk and spiral density waves driven into the disk. We see from the simulations that the disk is not only truncated by the binary but also can be compressed, causing a high gas density at the disk edge, resulting in the appearance of a gas ring.

We find that the outermost two spiral arms of the disk of HD 141569A are qualitatively reproduced by a perturbation from its nearby binary companion HD 141569B, HD 141569C, confirming the scenario proposed by Augereau & Papaloizou (2004). However, we find closer morphological correspondence with thinner disks ($h/r \sim 0.04$) and moderately, $e \sim 0.2$, but not highly eccentric orbits for the external binary with the binary located near the periapse of its orbit. Because a higher binary eccentricity has a similar effect on the morphology as a thicker disk, these two parameters are redundant, and we cannot exclude the possibility that the binary eccentricity is higher. Our simulation accounts for only some of the asymmetries in the inner region (200–300 AU). It matches reasonably well the position of the binary, and predicts an asymmetry in the outermost two arms that is seen in the disk of HD 141569A. However, our simulations also are not as lopsided as the observed disk and do not exhibit the high density on the southwestern side of the disk that was seen in the observations by Clampin et al. (2003). Our simulations do not do as good a job as the secular collisionless particle simulations of Augereau & Papaloizou (2004) at accounting for the lopsided shape of the disk edge, although those simulations do not exhibit outer spiral arms. Our simulations also fail to exactly match the shape of the outermost spiral features. We suspect that a three-dimensional simulation would be required to do this. Our simulations also exhibit an enhanced density at the disk edge (similar to that observed) and episodes of high accretion in the inner disk following the binary's close passage. In a planetesimal-dominated disk (rather than a hydrodynamic one), these episodes could correspond to episodes of increased collision and dust production (Kenyon & Bromley 2002).

The current uncertainty in the composition of these disks hampers our ability to simulate them. These disks are suspected to contain planetesimals, but collisions are also expected to be important over the lifetime of the disks. Here, we have opted to carry out two-dimensional hydrodynamic simulations as a first step. In future, three-dimensional particle simulations that include collisions would provide a better physical match to the suspected properties of debris disks. The simulations of Augereau & Papaloizou (2004) investigate long-timescale secular perturbations and suggest that much of the morphology of this disk has been caused by repeated encounters with the binary HD 141569B, HD 141569C. In contrast, our simulations suggest that some of the structure (the outer spiral arms) in the disk of HD 141569A has been caused by a recent encounter with the binary. From attempting to match the orientation of the tidally excited spiral arms, we infer that the binary HD 141569B, HD 141569C is near periapse and that the binary is on a prograde orbit. Our estimated location of the periapse differs from that predicted by Augereau & Papaloizou (2004). Future numerical work could attempt to account for both the outer spiral arms (as done here) as well as the disk edge structure (as better done by Augereau & Papaloizou 2004).

In the case of HD 100546, a low-mass planetary perturber in a circular orbit might cause a low-amplitude two-armed spiral structure that is more open at larger radii than smaller radii. However, to match the observed spiral amplitude, $\sim$15%, the bound object must have a mass greater than $M > 0.02\ M_\odot$, in contradiction to the limits placed by the lack of detection of possible associated objects in the NICMOS and STIS images of Grady et al. (2001) and Augereau et al. (2001; $M \lesssim 0.01\ M_\odot$ if the object is the same age as HD 100546). A recent stellar encounter might also be responsible for the spiral structure. Our simulations suggest that a star of mass about 0.1 $M_\odot$ passing within 600 AU of HD 100546 within a few thousand years ago could account for the spiral structure. The timescale since the encounter is long enough that the star could be outside the field

of view of the STIS and NICMOS images. However, we have failed to identify a candidate from the USNO-B catalog. The probability that a field star was responsible for the collision in the past few thousand years is very low, $\sim 10^{-6}$. If the star responsible for the encounter originated from a region (not yet identified) with a higher stellar density located within a few arcminutes of HD 100546, then the probability of the encounter might be higher.

Here we have discussed three scenarios that could account for the observed spiral structure in the disk of HD 100546. Only an extremely cold and thin disk could be unstable to the formation of spiral density waves. For the reasons discussed above, bound perturbers also provide unlikely explanations. This has left only the possibility that a recent stellar encounter caused the spiral structure; however, this scenario is highly improbable and the star responsible has not yet been identified. This implies that the observed spiral structure currently lacks a good explanation. A recent studies of the infrared spectral energy distribution of HD 100546 suggests that its outer edge is flared (Dullemond & Dominik 2004; Meeus et al. 2001). Consequently, structure observed in the visible bands could be due to variations in the vertical structure. Future scenarios for the disk of HD 100546 might consider flared disk models that exhibit variations in both vertical and azimuthal structure. Promising possibilities include transient spiral structure excited by planetesimal collisions (e.g., Kenyon & Bromley 2004).

The division between bound perturbers and flybys is important. While both excite spiral arms, a single flyby will not truncate the disk. However, an eccentric bound perturber, because it makes multiple close passages, is likely to truncate the disk. Notably, HD 141569A is an example of the second case, but previous studies have proposed that HD 100546 could be an example of the first case or a flyby. HD 100546 has a large disk extending out to 500 AU, past the location of the spiral structure. HD 100546 also has an envelope that extends out to 1000 AU (Grady et al. 2001). We expect that the process of disk truncation depends on the velocity of the perturber. If the perturber is moving fast, then an impulse approximation is appropriate and disk particles nearer the point of closest approach are more strongly affected than those on the opposite side, particularly if the object has low mass (Pfalzner 2003). In contrast, the repeated encounters of the binary HD 141569B, HD 141569C enforce a sharp outer disk boundary.

We note that the simulations presented here suffered from various restrictions. They were two-dimensional, making it impossible to investigate the three-dimensional structure of these disks. They suffered from artifacts caused by the boundary conditions. Future studies could be carried out in three dimensions. Larger grids could also be used, lessening the artifacts caused by the boundary. Three-dimensional simulations may provide a better match to the outer morphology of the disk of HD 141569A and make it possible to more tightly constrain its disk thickness and the companion's orbit. In the future, we also hope to simulate the effect of bound perturbers and flybys on disks containing planets, in search of explanations for the eccentric planets proposed to explain the structure of the disks of Vega, HR 4796A, and ϵ Eri (Wilner et al. 2002; Wyatt et al. 1999; Quillen & Thorndike 2002). The simulations carried out here were done using gaseous disks; however, these disks may contain massive planetesimals. While our flyby hydrodynamic simulations exhibit similar morphology to the collisionless simulations of Pfalzner (2003), future work that investigates the dynamics of disks containing both planetesimals that can collide and gas may be able to place constraints on the constituents of these disks from their morphology. Higher angular resolution and deeper imaging spanning additional wavelengths will also provide more constraints on the dynamical processes affecting these disks.

Since most stars are born in stellar clusters and are binaries, encounters may strongly influence forming planetary systems. We find here that the binary companion of HD 141569A has likely truncated and compressed its disk. Future close encounters will also excite spiral density waves in the disk. This type of excitation, taking place on timescales of thousands of years, could contribute to periodic episodes of high accretion in gaseous disks or high dust production in planetesimal disks. We note that flybys excite structure for only short periods of time, so future studies can search for and identify objects capable of perturbing young stellar disks.

Once the object responsible for exiting the spiral structure is identified, the nature of the encounter can be explored more quantitatively, and we expect that many of the free parameters affecting our simulations (such as orbit, disk thickness, boundary conditions, and disk composition) can be better constrained.

We thank Mike Jura, Dan Watson, Pawel Artymowicz, and Carol Grady for helpful discussions and comments. We thank F. Masset for his help and for providing the code. Support for this work was provided by NSF grants AST-0406823, AST-9702484, and AST-0098442, US Department of Energy grant DE-FG02-00ER54600, and the Laboratory for Laser Energetics. This material is based on work supported by NASA under grant NNG04GM12G issued through the Origins of Solar Systems Program and grant NAG5-8428. This research was supported in part by the National Science Foundation to the KITP under grant PHY99-07949.

REFERENCES

Adams, F. C., & Laughlin, G. 2001, Icarus, 150, 151
Artymowicz, P., & Lubow, S. H. 1994, ApJ, 421, 651
Augereau, J. C., Lagrange, A. M., Mouillet, D., & Menard, F. 1999a, A&A, 350, L51
———. 2001, A&A, 365, 78
Augereau, J. C., Lagrange, A. M., Mouillet, D., Papaloizou, J. C. B., & Grorod, P. A. 1999b, A&A, 348, 557
Augereau, J. C., & Papaloizou, J. C. B. 2004, A&A, 414, 1153
Baraffe, I., Chabrier, G., Allard, F., & Hauschildt, P. H. 2002, A&A, 382, 563
Binney, J., & Tremaine, S. 1987, Galactic Dynamics (Princeton: Princeton Univ. Press)
Boffin, H. M. J., Watkins, S. J., Bhattal, A. S., Francis, N., & Whitworth, A. P. 1998, MNRAS, 300, 1189
Bouwman, J., de Koter, A., Dominik, C., & Waters, L. B. F. M. 2003, A&A, 401, 577
Brittain, S. D., & Rettig, T. W. 2002, Nature, 418, 57
Clampin, M., et al. 2003, AJ, 126, 385
Clarke, C. J., & Pringle, J. E. 1993, MNRAS, 261, 190
Corradi, W. J. B., Franco, G. A. P., & Knude, J. 1997, A&A, 326, 1215
Deleuil, M., Lecavelier des Etangs, A., Bouret, J.-C., Roberge, A., Vidal-Madjar, A., Martin, C., Feldman, P. D., & Ferlet, R. 2004, A&A, 418, 577
Dullemond, C. P., & Dominik, C. 2004, A&A, 417, 159
Fukagawa, M., et al. 2004, ApJ, 605, L53
Goldreich, P., & Sari, R. 2003, ApJ, 585, 1024
Goldreich, P., & Tremaine, S. 1980, ApJ, 241, 425
Grady, C. A., Sitko, M. L., Bjorkman, K. S., Perez, M. R., Lynch, D. K., Russell, R. W., & Hanner, M. S. 1997, ApJ, 483, 449
Grady, C., et al. 2001, AJ, 122, 3396
Henry, A. L., Quillen, A. C., & Gutermuth, R. 2003, AJ, 126, 2831
Hu, J. Y., Thé, P. S., & de Winter, D. 1989, A&A, 208, 213

Jayawardhana, R., Fisher, S., Hartmann, L., Telesco, C., Pina, R., & Giovanni, F. 1998, ApJ, 503, L79
Kalas, P., Deltorn, J.-M., & Larwood, J. 2001, ApJ, 553, 410
Kenyon, S. J., & Bromley, B. C. 2002, AJ, 123, 1757
———. 2004, AJ, 127, 513
Korycansky, D. G., & Papaloizou, J. C. B. 1995, MNRAS, 274, 85
Lada, C. J., & Lada, E. A. 2003, ARA&A, 41, 57
Larwood, J. D., & Kalas, P. G. 2001, MNRAS, 323, 402
Lecavelier des Etangs, A., et al. 2003, A&A, 407, 935
Li, A., & Lunine, J. L. 2003, ApJ, 594, 987
Lin, D. N. C., & Papaloizou, J. C. B. 1993, Protostars and Planets III, ed. E. Levy & J. I. Lunine (Tucson: Univ. Arizona Press), 749
Luhman, K. L., Stauffer, J. R., Muench, A. A., Rieke, G. H., Lada, E. A., Bouvier, J., & Lada, C. J. 2003, ApJ, 593, 1093
Malfait, K., Waelkens, C., Waters, L. B. F. M., Vandenbussche, B., Huygen, E., & de Graauw, M. S. 1998, A&A, 332, L25
Masset F. S. 2000, A&AS, 141, 165
———. 2002, A&A, 387, 605
Masset, F. S., & Papaloizou, J. C. B. 2003, ApJ, 588, 494
Meeus, G., Waters, L. B. F. M., Bouwman, J., van den Ancker, M. E., Waelkens, C., & Malfait, K. 2001, A&A, 365, 476
Monet, D., et al. 2003, AJ, 125, 984
Mouillet, D., Lagrange, A. M., Augereau, J. C., & Menard, F. 2001, A&A, 372, L61
Murray, C. D., & Dermott, S. F. 1999, Solar System Dynamics (Cambridge: Cambridge Univ. Press)
Pantin, E., Waelkens, C., & Lagage, P. O. 2000, A&A, 361, L9
Pfalzner, S. 2003, ApJ, 592, 986
Quillen, A. C., & Thorndike, S. 2002, ApJ, 578, L149
Savonije, G. J., Papaloizou, J. C. B., & Lin, D. N. C. 1994, MNRAS, 268, 13
Stone, J. M., & Norman, M. L. 1992, ApJS, 80, 753
van den Ancker, M. E., The, P. S., Tjin A Djie, H. R. E., Catala, C., de Winter, D., Blondel, P. F. C., & Waters, L. B. F. M. 1997, A&A, 324, L33
Varnière, P., Quillen, A. C., & Frank, A. 2004, ApJ, 612, 1152
Vieira, S. L. A., Pogodin, M. A., & Franco, G. A. P. 1999, A&A, 345, 559
Weinberger, A. J., Rich, R. M., Becklin, E. E., Zuckerman, B., & Matthews, K. 2000, ApJ, 544, 937
Weinberger, A. J., et al. 1999, ApJ, 525, L53
Wilner, D. J., Bourke, T. L., Wright, C. M., Jørgensen, J. K., van Dishoeck, E. F., & Wong, T. 2003, ApJ, 596, 597
Wilner, D. J., Holman, M. J., Kuchner, M. J., & Ho, P. T. P. 2002, ApJ, 569, L115
Wyatt, M. C., Dermott, S. F., Telesco, C. M., Fisher, R. S., Grogan, K., Holmes, E. K., & Pina, R. K. 1999, ApJ, 527, 918
Zuckerman, B., Forveille, T., & Kastner, J. H. 1995, Nature, 373, 494